JOC The Journal of Organic Chemistry

ARTICLE

pubs.acs.org/joc

Recognition of Polycyclic Aromatic Hydrocarbons and Their Derivatives by the 1,3-Dinaphthalimide Conjugate of Calix[4]arene: Emission, Absorption, Crystal Structures, and Computational Studies

Anilkumar Bandela,[†] Jugun Prakash Chinta,[†] Vijaya Kumar Hinge,[†] Amol G. Dikundwar,[‡] Tayur N. Guru Row,[‡] and Chebrolu P. Rao*[,†]

[†]Department of Chemistry, Indian Institute of Technology Bombay, Powai, Mumbai-400 076, India

[‡]Solid State and Structural Chemistry Unit, Indian Institute of Science, Bangalore-560 012, India

Supporting Information

ABSTRACT: Polycyclic aromatic hydrocarbons (PAHs) are environmental pollutants as well as well-known carcinogens. Therefore, it is important to develop an effective receptor for the detection and quantification of such molecules in solution. In view of this, a 1,3-dinaphthalimide derivative of calix[4]-arene (**L**) has been synthesized and characterized, and the structure has been established by single crystal XRD. In the crystal lattice, intermolecular arm-to-arm $\pi\cdots\pi$ overlap dominates and thus **L** becomes a promising receptor for providing interactions with the aromatic species in solution, which can be monitored by following the changes that occur in its fluorescence and absorption spectra. On the basis of the solution studies carried out with about 17 derivatives of the aromatic guest molecular systems, it may be concluded that the changes that occur in the fluorescence intensity seem to be proportional to the number of aromatic rings present and thus proportional to the extent of $\pi\cdots\pi$ interaction present between the naphthalimide moieties and the aromatic portion of the guest molecule. Though the nonaromatic portion of the guest species affects the fluorescence quenching, the trend is still based on the number of rings present in these. Four guest aldehydes are bound to **L** with K_{ass} of 2000−6000 M^{-1} and their minimum detection limit is in the range of 8−35 μM. The crystal structure of a naphthaldehyde complex, **L.2b**, exhibits intermolecular arm-to-arm as well as arm-to-naphthaldehyde $\pi\cdots\pi$ interactions. Molecular dynamics studies of **L** carried out in the presence of aromatic aldehydes under vacuum as well as in acetonitrile resulted in exhibiting interactions observed in the solid state and hence the changes observed in the fluorescence and absorption spectra are attributable for such interactions. Complex formation has also been delineated through ESI MS studies. Thus **L** is a promising receptor that can recognize PAHs by providing spectral changes proportional to the aromatic conjugation of the guest and the extent of aromatic $\pi\cdots\pi$ interactions present between **L** and the guest.

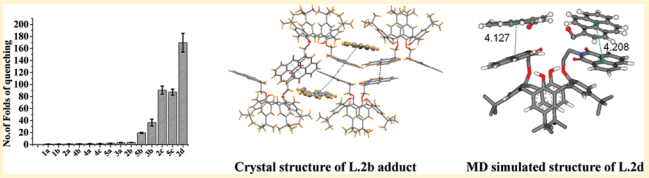

INTRODUCTION

Polycyclic aromatic hydrocarbons (PAHs) possess condensed benzene structures. These are widespread organic environmental pollutants formed during the incomplete combustion of carbon-containing fuels apart from their occurrence in natural crude oil, fossil fuels, and coal deposits.[1] PAHs are known to be hazardous for human kind because of their carcinogenic and mutagenic properties.[2−8] Owing to their lipophilic nature, their solubility in water is very poor and hence they persist in the environment for a longer period.[9−11] However, these are degraded by microbials by way of conversion to some of their oxidative products and hence become soluble. So it is important to find effective receptors to detect these even at low concentrations.[12−20] In this regard, calixarenes are of interest because of their preformed cavities, well-organized binding cores, and also for the presence of hydrophobic moieties. By appropriate derivatization, calix-[4]arene can be made as a selective host for different guest ions and molecules. In the literature Raman spectroscopy and chromatography methods have been employed for the detection of PAHs.[21−23] Though there are few reports on silver nanoparticles of the functionalized calix[4]arene[24−26] for the detection of PAHs, to our knowledge there are no reports on the selective recognition of PAHs by any calixarene derivative in solution using absorption and emission spectroscopy techniques, and hence the present study. Recently, our group was involved in synthesizing several calix[4]arene derivatives and studying their ion and molecular (amino acids) recognition properties.[27−35] Thus, in this paper, synthesis and characterization of a naphthalimide calix[4]arene conjugate **L** has been reported and studied for its interaction toward polycyclic aromatic hydrocarbons and their related molecules by spectroscopy, crystallography, and computational methods.

RESULTS AND DISCUSSION

The receptor 1,3-dinaphthalimide functionalized calix-[4]arene (**L**) has been synthesized by going through several steps starting from *p-tert*-butylcalix[4]arene (**1**) followed by

Received: December 2, 2010
Published: February 11, 2011

   dx.doi.org/10.1021/jo1023409 | *J. Org. Chem.* 2011, 76, 1742–1750

Scheme 1. Synthesis of L[a]

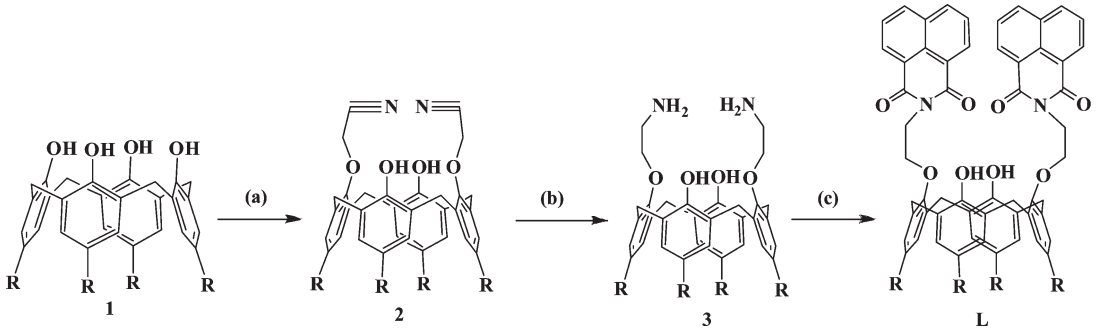

[a] Reagents and conditions: (a) K_2CO_3, NaI, $ClCH_2CN$, dry acetone, reflux for 12 h. (b) $LiAlH_4$, dry THF, reflux for 7 h. (c) Naphthalic anhydride, dry C_2H_5OH, reflux for 12 h. R = *t*-Bu.

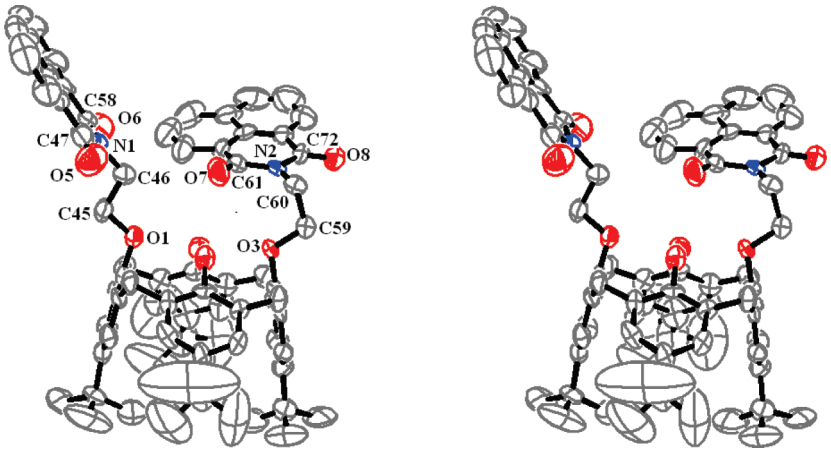

Figure 1. Stereo view of the molecular structure as obtained from the single crystal XRD of **L**.

dinitrile (**2**) and then the diamine (**3**) derivative and the reaction of **3** with naphthalic anhydride in dry ethanol as shown in Scheme 1.[27,36] The precursors and final products were characterized by analytical and spectral techniques (Experimental Section, Supporting Information, SI 01).

The receptor molecule **L** has been characterized by ^1H and ^{13}C NMR, IR, ESI MS, and elemental analysis. The protons of the bridged methylene appear at 3.28 and 4.34 ppm owing to the diastereotopic coupling with a coupling constant of 13.2 Hz indicating the cone conformation. **L** was studied for the recognition of compounds possessing a varying number of aromatic rings through fluorescence and UV−visible spectroscopy. The structure of **L** and its complex with naphthaldehyde (**L.2b**) have been established by single crystal XRD.

Structure of L. Single crystals of **L** were grown from chloroform solution by slow evaporation and the diffraction data were collected at 120 K on OXFORD DIFFRACTION XCALIBUR-S. **L** crystallizes in the monoclinic system with space group $P2_1/n$ ($Z = 4$) by accepting one chloroform molecule per one unit of the complex as solvent of crystallization. Preliminary data of diffraction, structure determination, and refinement are given in the SI, section 02. The single crystal XRD structure of **L** exhibits cone conformation for the calixarene as the lower rim intramolecular circular hydrogen bonding is being retained (Figure 1). The cone conformation persists even in the solution as is evident from the ^1H NMR spectrum. The corresponding dihedral angles of the two arms were found to be different except for C45−C46−N1−C58 = C59−C60−N2−C72 = −86.5°. Interestingly, the naphthalimide moiety of one of the arms lies almost perpendicular to the principal axis of the calixarene platform, while the other is in a parallel orientation. In the lattice, four units of **L** come closer wherein two of these extend one of their arms in such a way that there exists a $\pi\cdots\pi$ stacking of naphthalimide moieties disposed at a distance of 3.678 Å (Figure 2). All this results in a well-organized channel-like molecular architecture that is well poised for trapping aromatic guest molecules by using the hydrophobic regions formed between calix-conjugate units (Figure 2).

Fluorescence Titration of L. **L** has been titrated with different aromatic derivatives shown in Chart 1. The choice for such molecules arises from the point of view of understanding the effect of ring size (one or more aromatic rings) and substitution(s) on fluorescence quenching of **L**.

The titrations were carried out in acetonitrile by exciting the solutions at 334 nm and measuring the emission intensity in the range 344 to 550 nm. The studies were carried out by maintaining the concentration of **L** at 10 μM throughout the experiment and varying the mole ratio of the added guest molecule. As the emission has some contribution from the added guest, like what happens in the case of the anthracenyl moiety (the emission intensity is indeed low when the guest molecule is bound to −CHO or −OH), corresponding emission of the guest species was subtracted before analyzing the data quantitatively. While the subtraction was done in every case, a representative titration in

dx.doi.org/10.1021/jo1023409 |*J. Org. Chem.* 2011, 76, 1742–1750

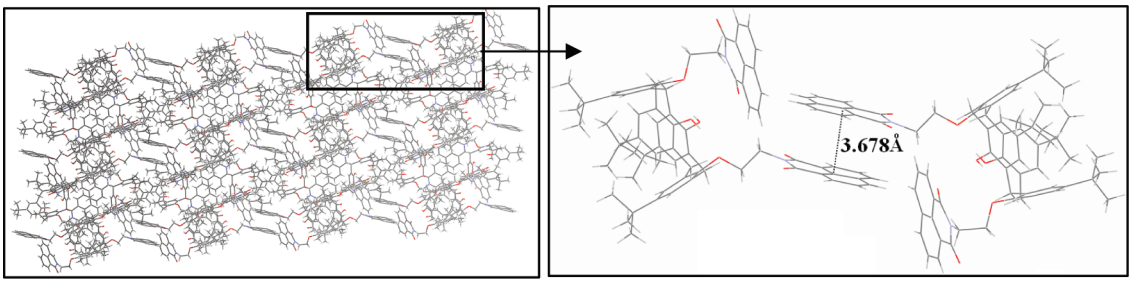

Figure 2. Crystal packing diagram of **L**.

Chart 1. Aromatic Hydrocarbons and Their Derivatives (5a, 5b, 5c, 6b, 6c)[a] Used in the Fluorescence and Absorption Studies

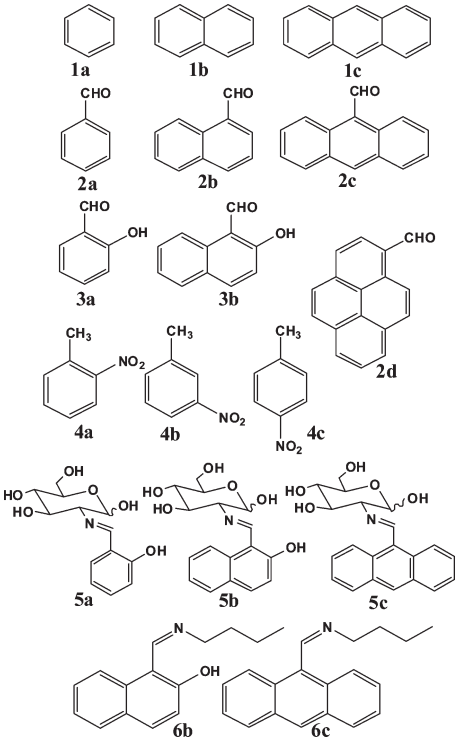

[a]**5a**: 1-(D-glucopyranosyl-2-deoxy-2-iminomethyl)-2-hydroxybenzene (Glu-2-SI). **5b**: 1-(D-glucopyranosyl-2-deoxy-2-iminomethyl)-2-hydroxy-napthalene (Glu-2-NI). **5c**: 1-(D-glucopyranosyl-2-deoxy-2-iminomethyl)-anthracene (Glu-2-AI). **6b**: *N*-(2-hydroxynapthylid-2-ine)butylamine (BNI). **6c**: *N*-(2-hydroxyanthracenylid-2-ine)butylamine (BAI).

the case of **1c** has been shown in Figure 3. The emission band observed at 378 nm for **L** gradually decreases as the concentration of the added guest species increases. Representative titration results were shown in the case of **2c** (Figure 4a). The number of folds of quenching observed at saturation has been shown in Figure 4b for all the cases and the histogram clearly suggests significant quenching in the case of the guests possessing aromatic moiety. The quenching is higher when this is the anthracenyl or pyrenyl moiety. Thus the extent of fluorescence quenching by different guests has the following order: pyrenyl- > anthracenyl- ≫ naphthyl- > phenyl-. The fluorescence quenching is high by ∼4- to 5-fold on going from phenyl to naphthyl and ∼20-fold high on going from naphthyl to anthracenyl and it is only 2-fold on going from the anthracenyl to the pyrenyl moiety. All these results suggest that for the recognition, at least a naphthyl or higher size aromatic moiety should be present in the guest species.

Effect of aromatic ring size on fluorescence quenching: The quenching of the 378 nm emission band follows a trend, pyrenaldehyde (**2d**) ≫ Glu-2-AI (**5c**) ∼ 9-anthraldehyde (**2c**) ≫ 2-hydroxy naphthaldehyde (**3b**) > Glu-2-NI (**5b**) > naphthaldehyde (**2b**) ≈ salicilaldehyde (**3a**) ≈ Glu-2-SI (**5a**) ≥ substituted phenyl derivatives as well some unsubstituted aromatic molecules (Figure 4b and SI, section 04). Thus while phenyl derivatives exhibit minimal quenching, those of anthracenyl and pyrenyl derivatives exhibit very high quenching, and hence it is possible to quantify guests possessing anthracenyl or higher aromatic moiety. Among the aromatic aldehydes, the fluorescene quenching efficiency has the following trend: **2a** ≪ **2b** < **2c** < **2d** (Figure 5b), suggesting that as the size of the aromatic ring increases the fluorescence quenching ability also increases. A similar trend was observed in the fluorescence quenching of **L**, even among the aromatic glucosyl derivatives (**5a** ≪ **5b** < **5c**) (Figure 5c), supporting that the size of the aromatic ring plays a role in quenching the fluorescence, since the bigger aromatic moieties are expected to have greater $\pi\cdots\pi$ interactions. The presence of $\pi\cdots\pi$ interactions between **L** and the guest molecule has been shown in this paper based on absorption, crystal structure of **L.2b**, and computational studies. Fluorescence quenching has indeed been attributed to the presence of $\pi\cdots\pi$ interactions in the literature.[37,38] On the basis of our study, it may be noted that the increase in quenching is ∼5-fold on going from phenyl to naphthyl and about ∼3-fold on going from naphthyl to anthracenyl and ∼2-fold on going from anthracenyl to pyrenyl. Thus there is about a 30- to 35-fold increase in the quenching of fluorescence intensity on going from phenyl-based derivatives to those of the pyrenyl-based ones.

Effect of substituent on fluorescence quenching: The 378 nm emission band is not affected by the titration of **L** with simple aromatic guests, namely, benzene and naphthalene, but diminished when titrated with polar group attached derivatives, such as **2a** and **2b** (Figure 6). The presence of an electron-withdrawing group such as −OH on the aromatic ring increases the quenching of fluorescence of **L**. The **2a** shows minimal quenching in the fluorescence of **L** when compared to **3a**, which has an −OH group ortho to the aldehyde. Similarly, **2b** shows less quenching when compared to its −OH-substituted counterpart. Thus the extent of quenching seems to be dependent on both the ring size and the substituent present on the aromatic ring.

Fluorescence quenching of **L** is due to the transfer of electrons from the excited naphthlalimide moiety of the calix-conjugate

dx.doi.org/10.1021/jo1023409 |*J. Org. Chem.* 2011, 76, 1742–1750

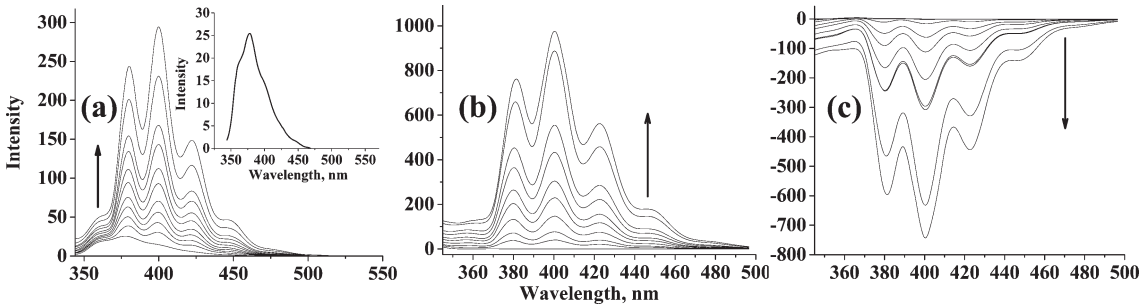

Figure 3. (a) Fluorescence spectra obtained during the titration of **L** with **1c** (inset: fluorescence spectrum of **L** in the absence of a guest molecule). (b) Fluorescence spectra obtained at similar concentrations of **1c** as in (a) as control. (c) Difference spectra obtained by subtracting (b) from the corresponding one in (a). Titrations were carried out between 6×10^{-4} M solution of **L** to result in a cuvette concentration of 10 μM and varied volumes of 6×10^{-4} M solution of **1c** to result in appropriate mole ratios.

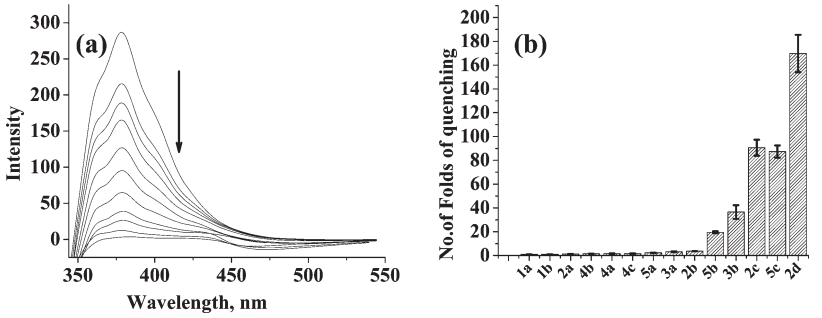

Figure 4. Fluorescence data for the titration of **L** by aromatic guests in acetonitrile: (a) Spectral traces obtained during the titration of **L** with **2c**. (b) Histogram representing the number of folds of quenching of fluorescence of **L** by various aromatic guests (refer to Chart 1). Titration details are the same as that given in the caption of Figure 3.

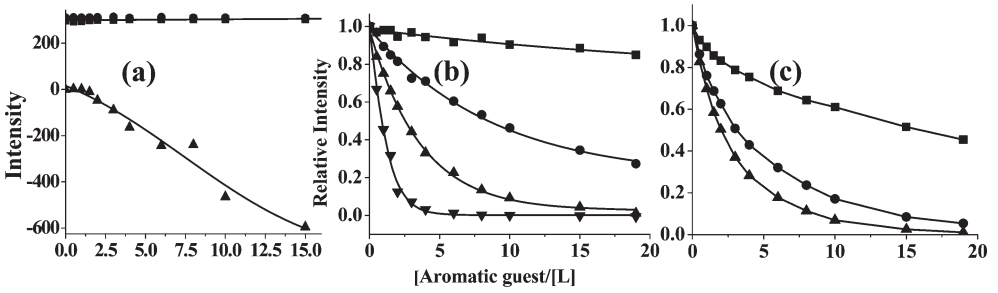

Figure 5. Plot of relative fluorescence intensity of **L** as a function of the mole equivalents of the aromatic guest molecules (refer to Chart 1): (a) **1a** (■), **1b** (●), and **1c** (▲); (b) **2a** (■), **2b** (●), **2c** (▲), and **2d** (▼); (c) **5a** (■, Glu-2-SI), **5b** (●, Glu-2-NI), and **5c** (▲, Glu-2-AI).

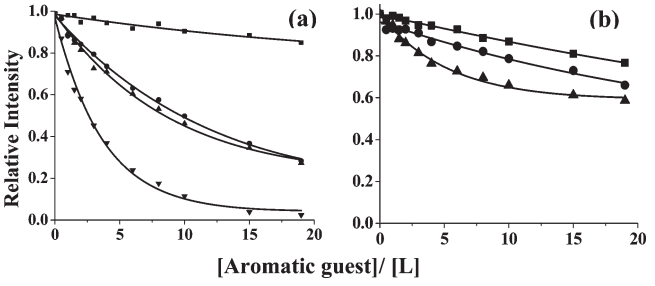

Figure 6. Plot of relative fluorescence intensity of **L** as a function of the mole equivalents of the guest molecule added: (a) hydroxy aromatic aldehydes, such as **2a** (■), **3a** (●), **2b** (▲), and **3b** (▼). (b) Nitro aromatic compounds, such as **4b** (■), **4a** (●), and **4c** (▲).

and then to the aromatic guest molecule that presumably is facilitated by the extent of $\pi\cdots\pi$ stacking and also due to some weak interactions present between the polar groups of the host−guest complex. Since benzene and its derivatives, such as **2a**, **3a**, **4a**, **4b**, and **4c**, are just phenyl-based ones, these affect the fluorescence of **L** to the least extent. The extent of quenching increases considerably as the aromatic ring size increases, resulting in a better stacking while the polar ends drive the molecule toward polar groups of **L**. Interactions of **2b** with **L** results in the formation of a 3:2 complex as analyzed by single crystal XRD and the results are reported in this paper. The moderate quenching observed in the case of **5b** and **3b** results from both stacking as well as the interactions present between the polar groups in the host−guest complex. All this is more pronounced in the case of

dx.doi.org/10.1021/jo1023409 |*J. Org. Chem.* 2011, 76, 1742–1750

Table 1. Stern−Volmer quenching constants for the titration of L with aromatic guest molecules

aromatic guest	K_{sv} (M^{-1})	aromatic guest	K_{sv} (M^{-1})
benzaldehyde (**2a**)	773(±87)	3-nitrotoulene (**4b**)	922(±96)
naphthaldehyde (**2b**)	7836(±183)	4-nitrotoulene (**4c**)	1026(±135)
anthraldehyde (**2c**)	37977(±1865)	2-nitrotoulene (**4a**)	1356(±110)
pyrenaldehyde (**2d**)	90118(±4021)	Glu-2-SI (**5a**)	3595(±170)
salicylaldehyde (**3a**)	6174(±411)	Glu-2-NI (**5b**)	21093(±57)
2-OH napthaldehyde (**3b**)	24586(±914)	Glu-2-AI (**5c**)	36478(±1572)
BNI (**6a**)	28552(±3228)	BAI (**6b**)	52000(±164)

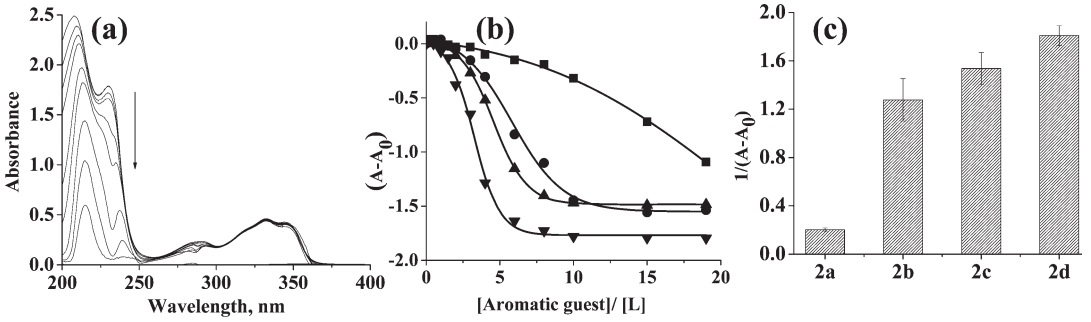

Figure 7. (a) Absorption spectral studies for the titration of **L** with pyrenaldehyde (**2d**) after subtracting the corresponding control. (b) Plot of absorbance of 230 nm band of **L** as a function of the mole equivalents of the aromatic aldehydes: ■, **2a**; ●, **2b**; ▲, **2c**; ▼, **2d**. (c) Histogram showing $1/(A - A_0)$ for the titration with the same aromatic aldehydes.

2c and **5c**, followed by **2d** owing to the increase in the size of the aromatic moiety. On the basis of the recognizable changes observed in fluorescence quenching, minimum detection limits for aromatic aldehydes were found to be 8.85 ± 0.05, 19.85 ± 0.15, and 33.8 ± 0.4 μM for **2d**, **2c**, and **2b**, respectively (SI, section 04). The Stern−Volmer quenching constants calculated were given in Table 1.

Absorption Titration of L by Aromatic Guest Molecules. Absorption titrations were carried out to support the results obtained from the fluorescence titrations and also to confirm the binding of the aromatic guest molecule with **L**. The absorbance of the 230 nm band decreases upon addition of the guest molecule, which is characteristic of the $\pi\cdots\pi$ interaction between **L** and the guest (Figure 7 and SI, section 05).[32] The extent to which the absorbance decreases follows a trend, i.e., pyrenyl > anthracenyl > naphthyl > phenyl, and this trend is the same as that observed from the fluorescence quenching studies. The association constants were found to be in the range 2500−6000 M^{-1}, with **2d** > **2c** > **2b** (could not be determined in the case of **2a**), indicating the presence of incremental levels of $\pi\cdots\pi$ interaction between **L** and aldehyde−guests owing to the size of the aromatic portion.

ESI-MS Studies. ESI-MS spectra of **L** treated with **2d** exhibited two very low abundance peaks, one at 1667 and the other at 1787, besides a major [1118 for {**L** + Na}, 100%] and a minor [1340 for{**L** + Na + *N*-alkylnaphthalimide fragment, 2.5%}] peak. Similar low abundance peaks are observed even in the case of other aldehyde−guests (**2b** and **2c**) except for **2a** (SI, section 06). The low abundance of the peaks arising for the complex may be attributable to the weak interactions proposed. The corresponding data have been given in Table 2.

Molecular Dynamics Studies. The **L** and aromatic aldehydes were optimized as explained in the Experimental Section and the structures obtained from B3LYP/6-31G have been used in simulation studies. MD studies were carried out to obtain

Table 2. ESI MS Studies of L with Aromatic Aldehydes

m/z	species assigned[a]
1667	{**L** + **X** + 1.5 × **2d**}
1787	{**L** + 3 × **2d**}
1687	{**L** + **X** + 2 × **2c**−CHO}
1778	{(**L**−H) + **X** + 2 × **2c** + 2Na}
1856	{**L** + 2 × **X** + 2 × **2b**}
1449	{**L** + **X** + **2b**−CHO}

[a] **X** = *N*-alkylnaphthalimide fragment with 224 mass units.

the structures of the complexes formed between **L** and aldehyde−guest under vacuum as well as in acetonitrile medium. In each case, except that of **2a**, mainly two aldehyde−guests were found to be interacting with the naphthalimide arms of **L**, at the end of 2 ns vacuum simulation. However, some aldehyde−guests were found to exhibit self-aggregation without interacting with **L** (Figure 8). From this outcome, all the noninteracting aromatic aldehydes were removed and those interacting with **L** (i.e., a 1:2 complex) were retained. At this stage, the complex was subjected to a 500 ps simulation under vacuum as well as in acetonitrile medium. At the end of these simulations, it was observed that some aldehyde−guests still interact with the naphthalimide arm of **L** (Figure 8). The results were found to be similar when these simulations were performed with **2b**, **2c**, and **2d**; however, no interacting **2a** was observed from the simulations carried out under vacuum or in acetonitrile. Indeed, the fluorescence of **L** was not quenched by titration with **2a**. The interaction of these aldehyde−guests is through $\pi\cdots\pi$ with a distance range of 3.6 to 4.2 Å and the percent of overlap observed follows the trend, **2d** > **2c** > **2b**, and the results reflect on the size of the aromatic moiety present in the guest. As compared to **2b**, the percent of overlap is 2-fold greater for **2d** and it is 1.5-fold greater for **2c**. All this is in line with what

dx.doi.org/10.1021/jo1023409 |*J. Org. Chem.* 2011, 76, 1742–1750

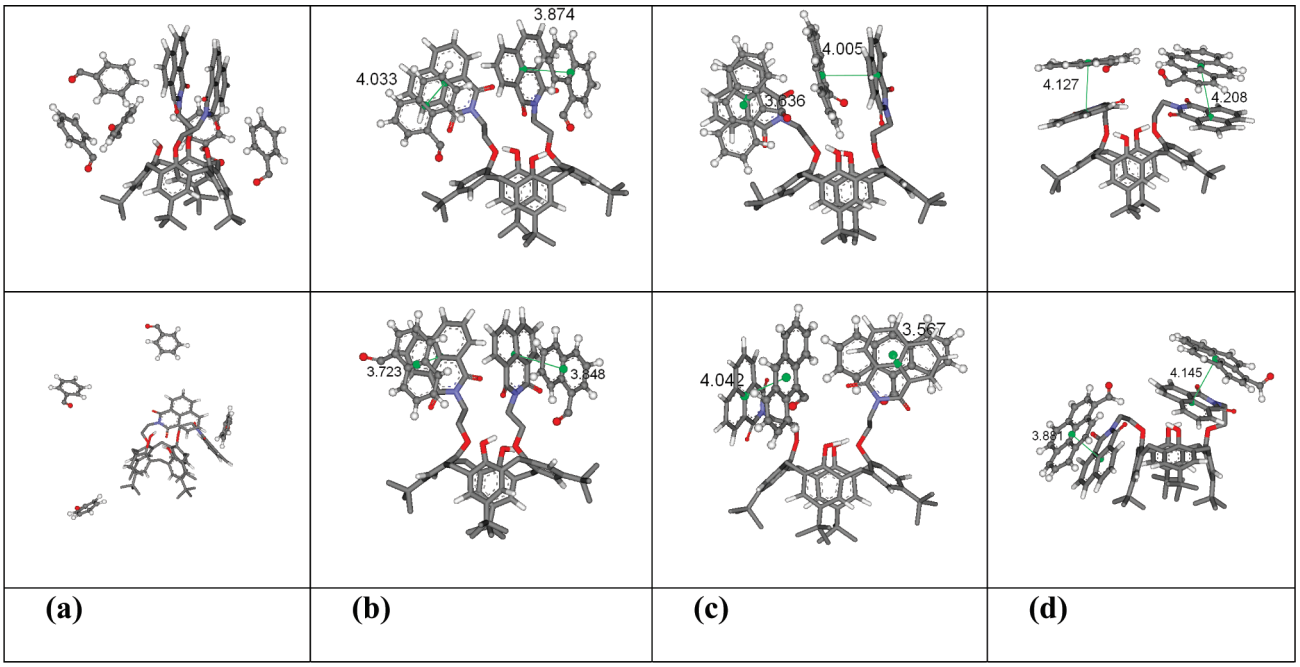

Figure 8. Structures obtained from 500 ps MD simulations of **L** carried out under vacuum (first row) and in acetonitrile (second row) in the presence of 2 molecules of aromatic aldehyde taken in a cubic box: (a) **2a**; (b) **2b**; (c) **2c**; and (d) **2d**.

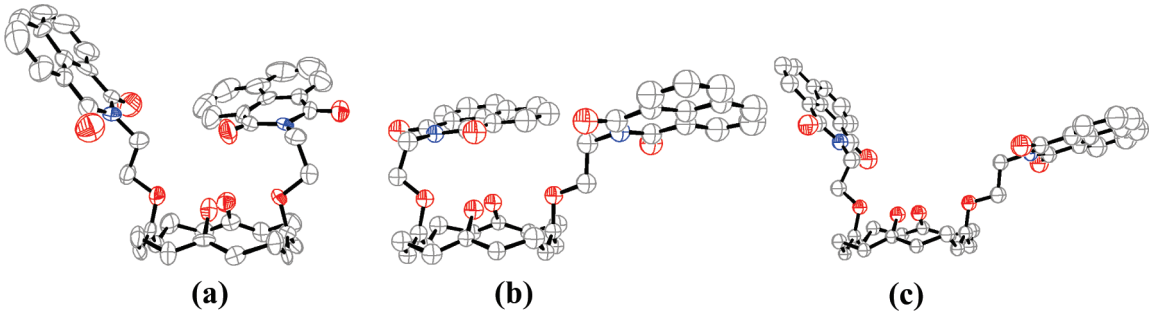

Figure 9. ORTEP diagrams of **L** drawn at 30% probability ellipsoids: (a) crystal structure of **L**, (b) naphthalimide side arms oriented on the same side from the crystal structure of **L** in the adduct of **L.2b**, and (c) naphthalimide side arms facing opposite to each other from the crystal structure of the adduct of **L.2b** (calix[4]arene cavity and hydrogen atoms have been removed for clarity).

was observed in the fluorescence quenching, e.g., **2d** > **2c** > **2b** ≫ **2a**. Such $\pi\cdots\pi$ interactions were noticed from the lattice structure of the complex formed between **L** and **2b**, as given in this paper.

Computational studies carried out under vacuum with 4 molecules of **L** and 12 molecules of **2b** resulted in species (SI, section 07) possessing $\pi\cdots\pi$ interactions between **2b** molecules (4.165 Å), one **2b** and the naphthalimide arm (**NI**) (3.8 to 4.0 Å), and between the **NI**s of the arms coming from two neighbor **L**s (3.9 to 4.7 Å). Interactions such as **NI**$\cdots$**NI** and **2b**$\cdots$**NI** were found in the crystal lattice of the complex of **L.2b** with distances being 3.7 to 4.1 Å, as reported in this paper.

Structure of the Complex of L.2b. Single crystals of the complex of **L.2b** suitable for X-ray diffraction were obtained from the mixture of chloroform and acetonitrile (1:1) by slow evaporation. Since the crystals were found to be unstable, the data collection was done under a stream of liquid nitrogen. **L.2b** crystallizes in a centrosymmetric triclinic system. The asymmetric unit is comprised of two molecules of **L** and three molecules of **2b**. Orientation of the **NI** side arms differs considerably among the two **L** molecules present in the asymmetric unit. In one **L**, both arms are oriented on the same side, whereas in the other, they are opposite each other (Figure 9).

In the lattice, **L** are arranged to form layers, where the two adjacent layers have opposite flow of direction. The arms are oriented to facilitate the intermolecular $\pi\cdots\pi$ stacking interactions of the **NI** units from the adjacent layers. The packing diagram (Figure 10) reveals the importance of these $\pi\cdots\pi$ stacking interactions in the formation of the **L.2b** adduct. Two of the three symmetry independent **2b** molecules are found to be arranged parallel to the **NI** units from the adjacent layers while the third one lies in a vertical way (along *c*-axis).

The parallel arrangement of **2b** molecules ensures the formation of aromatic $\pi\cdots\pi$ interactions with the corresponding **NI** units of the neighboring **L** (Figure 11, Table 3). It may be noted that the layered arrangement of the **2b** parallel to the **NI** units is quite intact because of the $\pi\cdots\pi$ stacking interactions whereas the vertically arranged **2b** molecules which do not show $\pi\cdots\pi$ stacking are loosely held. Indeed, these vertically arranged **2b**s could only be refined isotropically and the associated thermal parameters are significantly large. Complexation through $\pi\cdots\pi$

dx.doi.org/10.1021/jo1023409 |*J. Org. Chem.* 2011, 76, 1742–1750

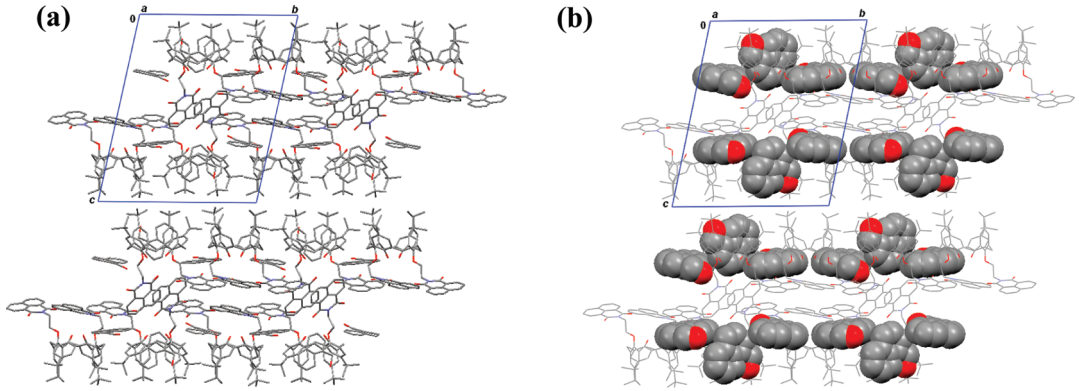

Figure 10. Packing diagrams of the complex **L.2b**: (a) layered arrangement of **L** molecules and (b) positions of **2b** molecules (shown as space filling model) in the crystal lattice of this adduct.

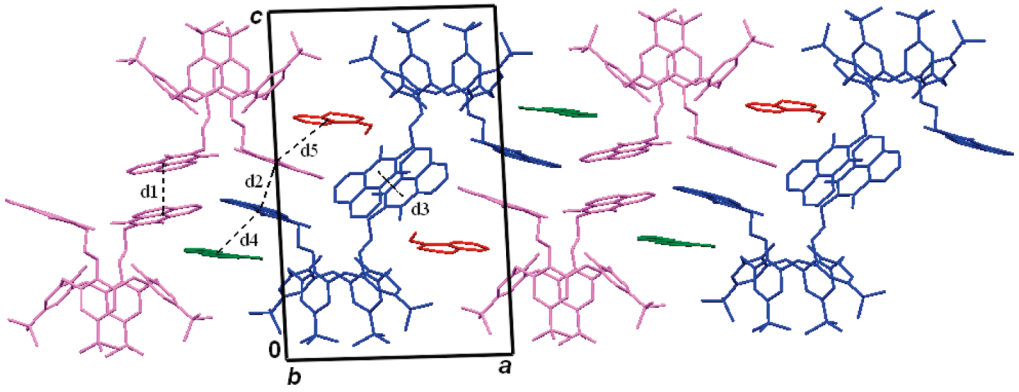

Figure 11. Packing diagram of **L** with **2b** viewed down the *b*-axis highlighting the presence of aromatic $\pi\cdots\pi$ stacking interactions in the adduct of **L.2b** (molecules in different colors indicate the symmetry independence). Note that vertically arranged **2b** molecules are not shown in the diagram for the purpose of clarity; d_1= 3.517 Å, d_2 = 3.721 Å, d_3 = 4.071 Å, d_4 = 3.942 Å, and d_5 = 3.658 Å.

Table 3. Intermolecular Aromatic $\pi\cdots\pi$ Interactions Observed in the Crystal Structure of the Complex L.2b

Cg···Cg[c]	symmetry code	*d*[Cg···Cg] (Å)	α (deg)[a]	slippage (Å)
Cg(1)···Cg(7)	1−*X*,2−*Y*,1−*Z*	3.4971 (d_1)[b]	1.88	
Cg(2)···Cg(12)	−*X*,2−*Y*,1−*Z*	3.7217 (d_2)[b]	2.00	
Cg(11)···Cg(11)	1−*X*,1−*Y*,1−*Z*	4.0687 (d_3)[b]	0.00	1.823
Cg(21)···Cg(20)	−*X*,1−*Y*,1−*Z*	3.9336 (d_4)[b]	13.10	
Cg(24)···Cg(9)	1+*X*,−1+*Y*,*Z*	3.6776 (d_5)[b]	15.05	
Cg(2)···Cg(20)	−*X*,2−*Y*,1−*Z*	3.7758	3.75	
Cg(2)···Cg(24)	−1+*X*,1+*Y*,*Z*	4.0679	14.49	
Cg(7)···Cg(7)	1−*X*,2−*Y*,1−*Z*	3.8518	0.00	1.717
Cg(7)···Cg(8)	1−*X*,2−*Y*,1−*Z*	3.9716	1.54	
Cg(9)···Cg(12)	−*X*,2−*Y*,1−*Z*	3.7066	4.01	
Cg(9)···Cg(24)	−1+*X*,1+*Y*,*Z*	3.6776	15.05	

[a] α is a dihedral angle between planes of the two rings (deg). [b] Distances shown in Figure 11. [c] Centroids of the rings.

has been noticed from three different crystal structures of dinuclear-Pt(II)-diazapyrenium-based metallacycle with PAHs as reported recently in the literature.[39]

CONCLUSIONS AND CORRELATIONS

The receptor calix[4]arene conjugate derivatized with 1,3-dinaphthalimide arms (**L**) has been synthesized and was characterized by analytical and spectral methods. The structure of **L** has been established by single crystal XRD. The naphthalimide moiety of one of the arms lies almost perpendicular to the imaginary principal axis of the calixarene platform, while the other is in a parallel orientation. **L** has been studied for the recognition of aromatic guest molecules by fluorescence and absorption spectroscopy. The fluorescence of **L** is quenched upon the addition of the guest species. The quenching is higher in the case of the guests possessing aromatic moiety, and follows a trend, pyrenaldehyde (**2d**) ≫ Glu-2-AI (**5c**) ≈ 9-anthraldehyde (**2c**) ≫ 2-hydroxynaphthaldehyde (**3b**) > Glu-2-NI (**5b**) > naphthaldehyde (**2b**) ≈ salicilaldehyde (**3a**) ≈ Glu-2-SI (**5a**) ≥ substituted phenyl derivatives as well some unsubstituted aromatic molecules. Benzaldehyde (**2a**) shows minimal quenching in the fluorescence of **L** as compared to **3a**, which has a −OH group ortho to the aldehyde. A similar trend was found between **2b** and **3b**. However, the glucosyl-substituted derivative **5a** shows quenching similar to that of its aldehyde precursor, **3a**. Similar trends were observed for **5b** vs **3b** and **5c** vs **2c**. Hence, the extent of quenching is dependent on both the ring size as well as the nature of the substituent present. Thus for the detection, at least a naphthyl moiety and a polar group are required, whereas the anthracenyl and higher PAHs are recognized to almost equal extent. The minimum concentration that can be detected was found to be 8.85 ± 0.05, 19.85 ± 0.15, and 33.8 ± 0.4 μM for **2d**, **2c**, and **2b**, respectively. The proposed interactions between **L** and aromatic guest have been shown in Figure 12.

dx.doi.org/10.1021/jo1023409 |*J. Org. Chem.* 2011, 76, 1742–1750

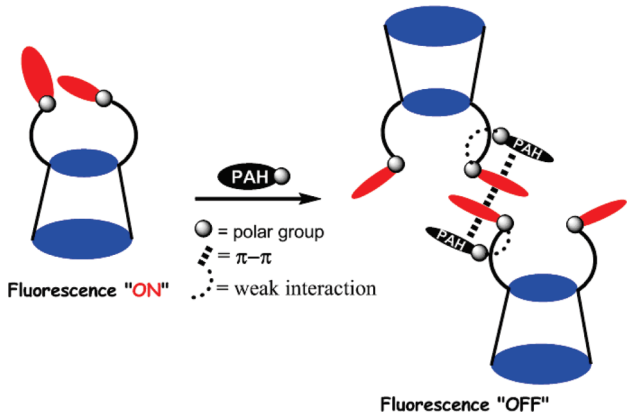

Figure 12. Proposed mode of interaction between **L** and aromatic guest molecule.

The absorption studies showed a decrease in the absorbance of the 230 nm band upon addition of a guest molecule, a trend that has been generally seen when even $\pi\cdots\pi$ interactions can set in. The extent of $\pi\cdots\pi$ interactions present between **L** and guests follows a trend, i.e., pyrenyl > anthracenyl > naphthyl > phenyl, and this trend is the same as that observed in the fluorescence quenching studies. On the basis of the absorption spectral changes, the association constants were found to be in the range of 2500−6000 M^{-1}. ESI-MS studies of **L** with aromatic aldehydes showed the presence of complexes formed between **L** and a guest molecule. Molecular dynamics studies carried out between **L** and aromatic aldehydes under vacuum as well as in acetonitrile medium showed the interaction of aromatic aldehydes with **L**, and these are primarily through $\pi\cdots\pi$ type interactions. These interactions were found to be stronger in the case of aromatic aldehydes having more rings. The percent of overlap observed between aromatic aldehyde and the naphthalimide arm varies as **2d** > **2c** > **2b**, suggesting that the extent of overlap is dependent on the size of the aromatic ring. Similar studies carried out with 4 molecules of **L** with 12 molecules of **2b** showed $\pi\cdots\pi$ interactions between two **2b**s, one **2b**, and the **NI**-arm, and between the **NI**-arms coming from two neighbor **L**s. Similar types of interactions were also found to be present in case of the crystal structure of the **L.2b** adduct. Thus **L** can be employed as a potential molecule for the analytical detection and quantification of environmental pollutants of anthracenyl and higher aromatics.

EXPERIMENTAL SECTION

Materials. All the aromatic compounds used in the titrations were obtained from local sources except for the glyco-conjugates which were synthesized in our lab. All the solvents used were dried and distilled by usual procedures before use. The elemental analysis, FTIR, absorption and emission, and ^{1}H and ^{13}C NMR and ESI MS were measured. Single crystal X-ray diffraction data were also measured for **L** and its complex with naphthaldehyde.

Synthesis and Characterization Data for the Receptor Molecule L. **L** has been synthesized in three steps on going from simple *p-tert*-butylcalix[4]arene (**1**) to give a dinitrile (**2**) followed by the diamine (**3**) as reported by us and others in the literature (Scheme 1).[27,36] To a mixture of **3** (1.5 g, 2.04 mmol) in dry ethanol (150 mL) was added naphthalic anhydride (1.01 g, 5.09 mmol) with stirring and the mixture was heated at reflux for 12 h under nitrogen atmosphere. The product was settled upon cooling the reaction mixture and was separated by filtration and dried under vacuum. The product was purified by chromatographic column filled with silica gel and was eluted with a mixture of dichloromethane and methanol (98:2) to give a yield of 1.45 g (65%). ^{1}H NMR ($CDCl_3$, δ ppm) 0.82 (s, 18H, $C(CH_3)_3$), 0.88 (s, 18H each, $C(CH_3)_3$), 3.28 (d, 4H, Ar-CH_2-Ar, J = 13.2 Hz), 4.28 (t, 4H, CH_2-CH_2, J = 7.2 Hz), 4.34 (d, 4H, Ar-CH_2-Ar, J = 13.2 Hz), 4.93 (t, 4H, CH_2-CH_2−, J = 7.3 Hz), 6.70 (s, 4H, Ar-*H*), 6.86 (s, 2H, Ar-O*H*), 6.98 (s, 4H, Ar-*H*), 7.76 (t, 2H, napthalimide, J = 7.3 Hz), 8.17 (d, 1H, napthalimide, J = 8.1 Hz), 8.68 (d, 1H, napthalimide, J = 7.3 Hz); ^{13}C NMR ($CDCl_3$, 100 MHz, δ ppm) 31.1, 31.8, 31.7, 33.9, 34.0, 39.6, 72.1, 122.6, 125.0, 125.6, 127.0, 127.9, 128.3, 131.5, 131.7, 132.4, 134.1, 141.2, 146.8, 150.0, 150.7, 164.2; ESI-MS m/z 1118 $[M + Na]^+$, 100%. Anal. Calcd for $C_{74}H_{82}N_2O_{10}$: C, 76.66, H, 7.13, N, 2.42. Found: C, 76.24, H, 6.92, N, 2.53.

Fluorescence and Absorption Titrations. Fluorescence emission spectra were measured on a Perkin-Elmer LS55 by exciting the samples at 334 nm and the emission spectra were recorded in the 344−550 nm range. The bulk solutions of **L** and aromatic guest molecules were prepared in CH_3CN in which 100 μL of $CHCl_3$ was used for dissolving **L**. Bulk solution concentration of **L** and aromatic guest molecules were maintained at 6×10^{-4} M. All the measurements were made in a 1 cm quartz cell and maintained the effective cuvette concentration of **L** as 10 μM in all the titrations. During the titration, the concentration of aromatic guest molecules was varied accordingly in order to result in the requisite mole ratios of these to **L** by taking a fixed volume of solvent and varying volumes of the solution of the guest molecule. The total volume of the solution used for the fluorescence measurements was maintained constant at 3 mL in all cases by simply adding the requisite volume of acetonitrile as the making up solvent. Appropriate background subtractions have been done wherever required. The solutions used for the fluorescence experiments have been used even for absorption titrations.

Computational Modeling. The starting models for **L**, **2a**, **2b**, **2c**, and **2d** were modeled computationally by using the Gaussian G03 package[40] at the B3LYP/6-31G level and were used in the present study. The initial coordinates for **L** were taken from our single crystal XRD structure. The interactions were modeled by carrying out molecular dynamics (MD) simulations initially under vacuum and then followed by the same in acetonitrile solvent. All the simulations were carried out in a cubic box. The vacuum simulations were carried out for 2 ns with the mixture, viz., {**L** + 5 copies of the aromatic aldehyde}, wherein all are randomly placed. Noninteracting aromatic aldehydes are being removed from the output of the vacuum simulation and the resulting model has been subjected to 500 ps simulation upon filling the cubic box of dimension 1.63, 2.686, 2.339 nm^3 with acetonitrile (~4900 molecules). The MD simulations were performed with the GROMACS 4.0.5[41] software package, using the GROMOS96 43a1 force field under vacuum. In acetonitrile medium, the simulations were carried out under periodic boundary conditions. The DFT optimized aromatic aldehydes were manually placed around **L** in a random fashion, using an Accelrys DS visualizer. Force fields for **L** and aromatic aldehydes were generated by using a PRODRG2.5[42] server and were included in the topology file. The total contents of the system were then energy minimized for ~2000 steps with the Steepest Descent (SD) method[43] in the case of vacuum, followed by position restraint being applied for 50 ps in the case of the presence of the solvent, and were treated under NVT condition (T = 300 K) with the equation of motion being integrated by the leapfrog algorithm with a step size of 2 fs. At the time of carrying out the computations **L** and aromatic aldehydes were coupled separately to a v-rescale temperature bath. The electrostatic interactions were calculated by using the particle Mesh Ewald summation method.[44] All bond lengths were constrained by using the LINCS algorithm.[45]

■ ASSOCIATED CONTENT

Supporting Information. Characterization data of **L** (SI 01), crystallographic data of **L** (SI 02), crystallographic data of **L.2b** (SI 03), fluorescence spectral traces for titration of **L** with aromatic compounds (SI 04), absorption spectral traces for titration of **L** with aromatic compounds (SI 05), ESI-MS spectral studies of **L** with aromatic aldehydes (SI 06), and molecular dynamics simulation studies (SI 07). This material is available free of charge via the Internet at http://pubs.acs.org.

■ AUTHOR INFORMATION

Corresponding Author

*Phone: +91 22 2576 7162. Fax: +91 22 2572 3480. E-mail: cprao@iitb.ac.in.

■ ACKNOWLEDGMENT

C.P.R. acknowledges the financial support from DST, CSIR, and DAE-BRNS. Both C.J.P. and A.G.D acknowledges their CSIR for SRF. We thank Mr. Atanu Mitra for providing glycoconjugates.

■ REFERENCES

(1) Richter, H.; Howard, J. B. *Prog. Energy Combust. Sci.* **2000**, *26*, 565–608.
(2) Harvey, R. G. *Polycyclic Aromatic Hydrocarbons*; John Wiley & Sons: New York, 1997.
(3) Groopman, J. D.; Kensler, T. W. *Chem. Res. Toxicol.* **1993**, *6*, 764–770.
(4) Wenzl, T.; Simon, R.; Kleiner, J.; Anklam, E. *Trends Anal. Chem.* **2006**, *25*, 716–725.
(5) Van Gijssel, H. E.; Schild, L. J.; Watt, D. L.; Roth, M. J.; Wang, G. Q.; Dawsey, S. M.; Albert, P. S.; Qiao, Y. L.; Taylor, P. R.; Dong, Z. W.; Poirier, M. C. *Mutat. Res.* **2004**, *547*, 55–62.
(6) Falco, G.; Domingo, J. L.; Llobet, J. M.; Teixido, A.; Casas, C.; Muller, L. *J. Food Prot.* **2003**, *66*, 2325–2331.
(7) Guo, H.; Lee, S. C.; Chan, L. Y.; Li, W. M. *Environ. Res.* **2004**, *94*, 57–66.
(8) Li, D.; Jiao, L. *Int. J. Gastrointest. Cancer* **2003**, *33*, 3–13.
(9) Cerniglia, C. E. *Biodegradation* **1992**, *3*, 351–368.
(10) Edwards, N. T. *J. Environ. Qual.* **1983**, *12*, 427–441.
(11) Jacob, J.; Karcher, W.; Belliardo, J. J.; Wagstaffe, P. J. *Fresenius' J. Anal. Chem.* **1986**, *323*, 1–10.
(12) Dickert, F. L.; Besenbock, H.; Tortschanoff, M. *Adv. Mater.* **1998**, *10*, 149–151.
(13) Dickert, F. L.; Tortschanoff, M.; Bulst, W. E.; Fischerauer, G. *Anal. Chem.* **1999**, *71*, 4559–4563.
(14) Dickert, F. L.; Achatz, P.; Halikias, K. *Fresenius' J. Anal. Chem.* **2001**, *371*, 11–15.
(15) Kirsch, N.; Hart, J. P.; Bird, D. J.; Luxton, R. W.; Mc Calley, D. V. *Analyst* **2001**, *126*, 1936–1941.
(16) Kirsch, N.; Honeychurch, K. C.; Hart, J. P.; Whitcombe, M. J. *Electroanalysis* **2005**, *17*, 571–578.
(17) Salinas-Castillo, A.; Sanchez-Barragan, I.; Costa-Fernandez, J. M.; Pereiro, R.; Ballestreros, A.; Gonzalez, J. M.; Segura-Carretero, A.; Fernandez-Gutierrez, A.; Sanz-Mendel, A. *Chem. Commun.* **2005**, 3224–3226.
(18) Carlson, C. A.; Lloyd, J. A.; Dean, S. L.; Walker, N. R.; Edmiston, P. L. *Anal. Chem.* **2006**, *78*, 3537–3542.
(19) Luo, N.; Hatchett, D. W.; Rogers, K. R. *Electroanalysis* **2006**, *18*, 2180–2187.
(20) Lai, J. P.; Niessner, R.; Knopp, D. *Anal. Chim. Acta* **2004**, *522*, 137–144.
(21) Danyi, S.; Brose, F.; Brasseur, C.; Schneider, Y. J.; Larondelle, Y.; Pussemier, L.; Robbens, J.; De Saeger, S.; Maghuin-Rogister, G.; Scippo, M. L. *Anal. Chim. Acta* **2009**, *633*, 293–299.
(22) Purcaro, G.; Moret, S.; Conte, L. S. *J. Sep. Sci.* **2008**, *31* 3936–3944.
(23) Ishizaki, A.; Saito, K.; Hanioka, N.; Narimatsu, S.; Kataoka., H. *J. Chromatogr., A* **2010**, *1217*, 5555–5563.
(24) Leyton, P.; Domingo, C.; Sanchez-Cortes, S.; Campos-Vallette, M.; Garcia-Ramos, J. V. *Langmuir* **2005**, *21*, 11814–11820.
(25) Leyton, P.; Sanchez-Cortes, S.; Garcia-Ramos, J. V.; Domingo, C.; Campos-Vallette, M.; Saitz, C.; Clavijo, R. E. *J. Phys. Chem. B* **2004**, *108*, 17484–17490.
(26) Guerrini, L.; Garcia-Ramos, J. V.; Domingo, C.; Sanchez-Cortes, S. *Langmuir* **2006**, *22*, 10924–10926.
(27) Dessingou, J.; Joseph, R.; Rao, C. P. *Tetrahedron Lett.* **2005**, *46*, 7967–7971.
(28) Joseph, R.; Ramanujam, B.; Pal, H.; Rao, C. P. *Tetrahedron Lett.* **2008**, *49*, 6257–6261.
(29) Pathak, R. K.; Ibrahim, S. M.; Rao, C. P. *Tetrahedron Lett.* **2009**, *50*, 2730–2734.
(30) Joseph, R.; Ramanujam, B.; Acharya, A.; Khutia, A.; Rao, C. P. *J. Org. Chem.* **2008**, *73*, 5745–5758.
(31) Joseph, R.; Ramanujam, B.; Acharya, A.; Rao, C. P. *J. Org. Chem.* **2009**, *74*, 8181–8190.
(32) Jugun, P. C.; Acharya, A.; Kumar, A.; Rao, C. P. *J. Phys. Chem. B* **2009**, *113*, 12075–12083.
(33) Joseph, R.; Jugun, P. C.; Rao, C. P. *J. Org. Chem.* **2010**, *75*, 3387–3395.
(34) Pathak, R. K.; Dikundwar, A. G.; Guru Row, T. N.; Rao, C. P. *Chem. Commun.* **2010**, *46*, 4345–4347.
(35) Acharya, A.; Ramanujam, B.; Jugun, P. C.; Rao, C. P. *J. Org. Chem.* **2011**, *76*, 127–137.
(36) Zhang, W.-C.; Huang, Z.-T. *Synthesis* **1997**, 1073–1076.
(37) Dhar, G.; Bhaduri, A. *J. Biol. Chem.* **1999**, *274*, 14568–14572.
(38) Pramanik, A.; Bhuyan, M.; Das, G. *J. Photochem. Photobiol., A* **2008**, *197*, 149–155.
(39) Blanco, V.; Garcia, M. D.; Terenzi, A.; Pia, E.; Fernandez-Mato, A.; Peinador, C.; Quintela, J. M. *Chem.—Eur. J.* **2010**, *16*, 12373–12380.
(40) Frisch, M. J.; Trucks, G. W.; Schlegel, H. B.; Scuseria, G. E.; Robb, M. A.; Cheeseman, J. R.; Montgomery, J. A., Jr.; Vreven, T.; Kudin, K. N.; Burant, J. C.; Millam, J. M.; Iyengar, S. S.; Tomasi, J.; Barone, V.; Mennucci, B.; Cossi, M.; Scalmani, G.; Rega, N.; Petersson, G. A.; Nakatsuji, H.; Hada, M.; Ehara, M.; Toyota, K.; Fukuda, R.; Hasegawa, J.; Ishida, M.; Nakajima, T.; Honda, Y.; Kitao, O.; Nakai, H.; Klene, M.; Li, X.; Knox, J. E.; Hratchian, H. P.; Cross, J. B.; Adamo, C.; Jaramillo, J.; Gomperts, R.; Stratmann, R. E.; Yazyev, O.; Austin, A. J.; Cammi, R.; Pomelli, C.; Ochterski, J. W.; Ayala, P. Y.; Morokuma, K.; Voth, G. A.; Salvador, P.; Dannenberg, J. J.; Zakrzewski, V. G.; Dapprich, S.; Daniels, A. D.; Strain, M. C.; Farkas, O.; Malick, D. K.; Rabuck, A. D.; Raghavachari, K.; Foresman, J. B.; Ortiz, J. V.; Cui, Q.; Baboul, A. G.; Clifford, S.; Cioslowski, J.; Stefanov, B. B.; Liu, G.; Liashenko, A.; Piskorz, P.; Komaromi, I.; Martin, R. L.; Fox, D. J.; Keith, T.; Al-Laham, M. A.; Peng, C. Y.; Nanayakkara, A.; Challacombe, M.; Gill, P. M. W.; Johnson, B.; Chen, W.; Wong, M. W.; Gonzalez, C.; Pople, J. A. *Gaussian 03*, revision C.02; Gaussian, Inc., Wallingford, CT, 2004.
(41) Hess, B.; Kutzner, C.; van der Spoel, D.; Lindahl, E. *J. Chem. Theory Comput.* **2008**, *4*, 435–447.
(42) Schuettelkopf, W.; van Aalten, D. M. F. *Acta Crystallogr.* **2004**, *D60*, 1355–1363.
(43) Deift, P.; Zhou, X. *Ann. Math.* **1993**, *137*, 295–368.
(44) Darden, T.; York, D.; Pedersen, L. *J. Chem. Phys.* **1993**, *98*, 10089–10092.
(45) Hess, B.; Bekker, H.; Berendsen, H. J. C.; Fraaije, M. J. G. E. *J. Comput. Chem.* **1997**, *18*, 1463–1472.